Electronic Supplementary Information (ESI)

Luminescent Europium(III) and Terbium(III) Complexes of β-Diketonate and Substituted Terpyridine Ligands: Synthesis, Crystal Structures and Elucidation of Energy Transfer Pathways

Zafar Abbas,[a] Srikanth Dasari,[a] María J. Beltrán-Leiva,[b] Plinio Cantero-López,[b,c] Dayán Páez-Hernández,[b,c] Ramiro Arratia-Pérez,[b,c] Ray J. Butcher,[d] Ashis K. Patra*,[a]

[a]Department of Chemistry, Indian Institute of Technology Kanpur, Kanpur 208016, Uttar Pradesh, India

[b]Relativistic Molecular Physics (ReMoPh) Group, Ph.D. Program in Molecular Physical Chemistry, Universidad Andrés Bello, Av. República 275, Santiago 8370146, Chile

[c]Center of Applied Nanoscience (CANS), Facultad de Ciencias Exactas, Universidad Andrés Bello, Av. República 275, Santiago 8370146, Chile

[d]Department of Chemistry, Howard University, Washington DC 20059, USA

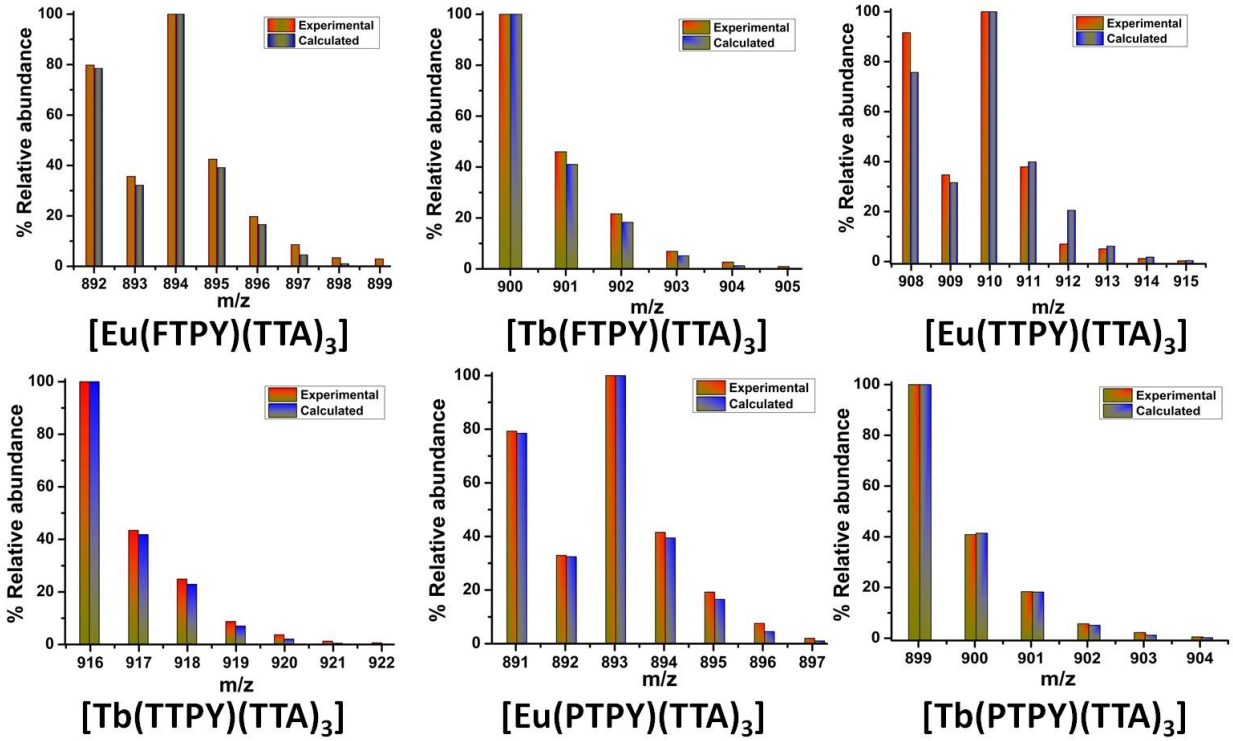

Figure S1.1.-S6.6 ESI-MS spectra with isotopic distribution for the parent ion peak of complexes **1-6** in DMF (Expanded region for molecular ion peaks in Figure S1-S6 given below)

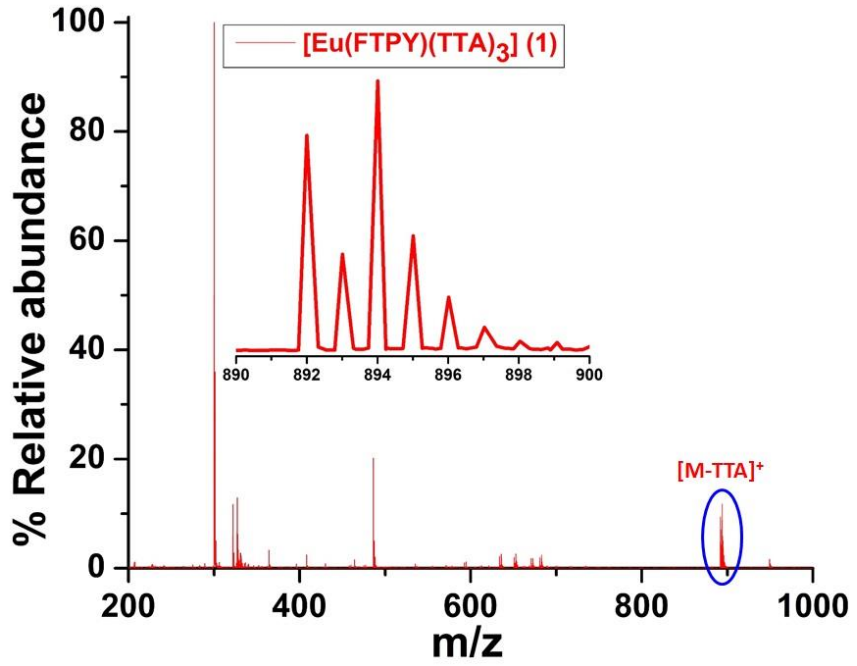

Figure S1. ESI-MS spectra with isotopic distribution for the parent ion peak of complex **1** in DMF.

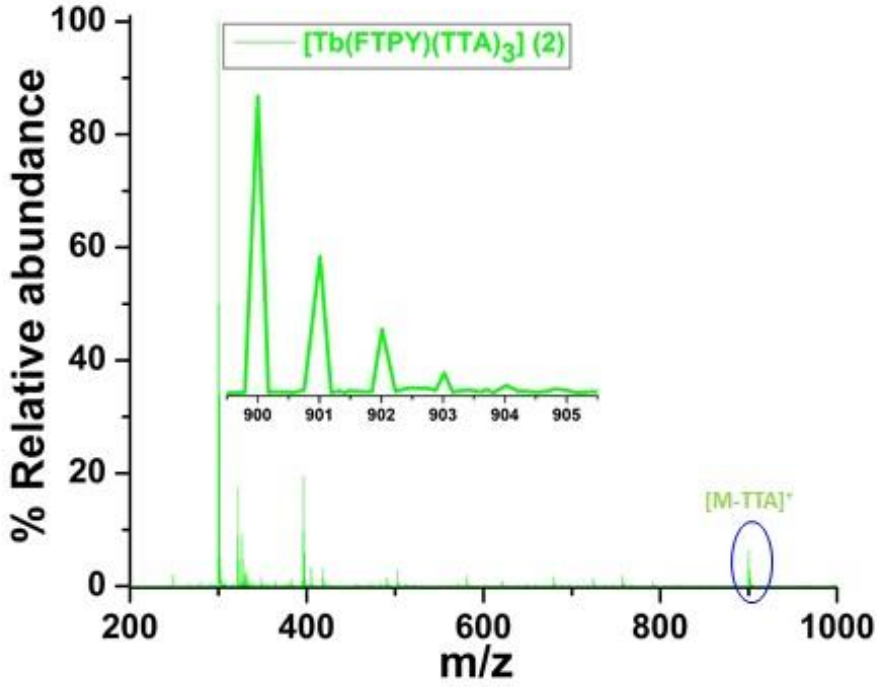

Figure S2. ESI-MS spectra with isotopic distribution for the parent ion peak of complex **2** in DMF.

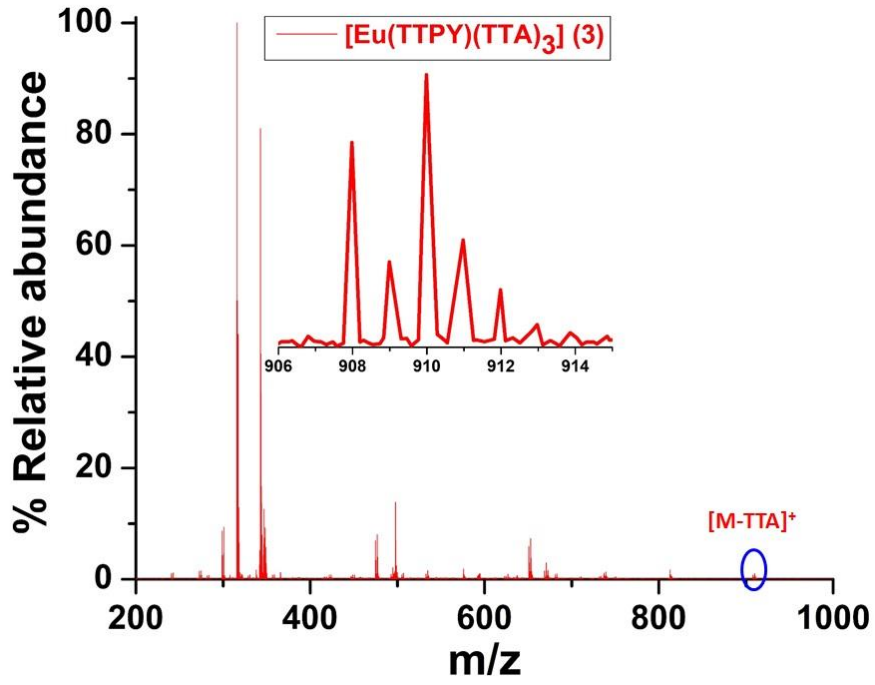

Figure S3. ESI-MS spectra with isotopic distribution for the parent ion peak of complex **3** in DMF.

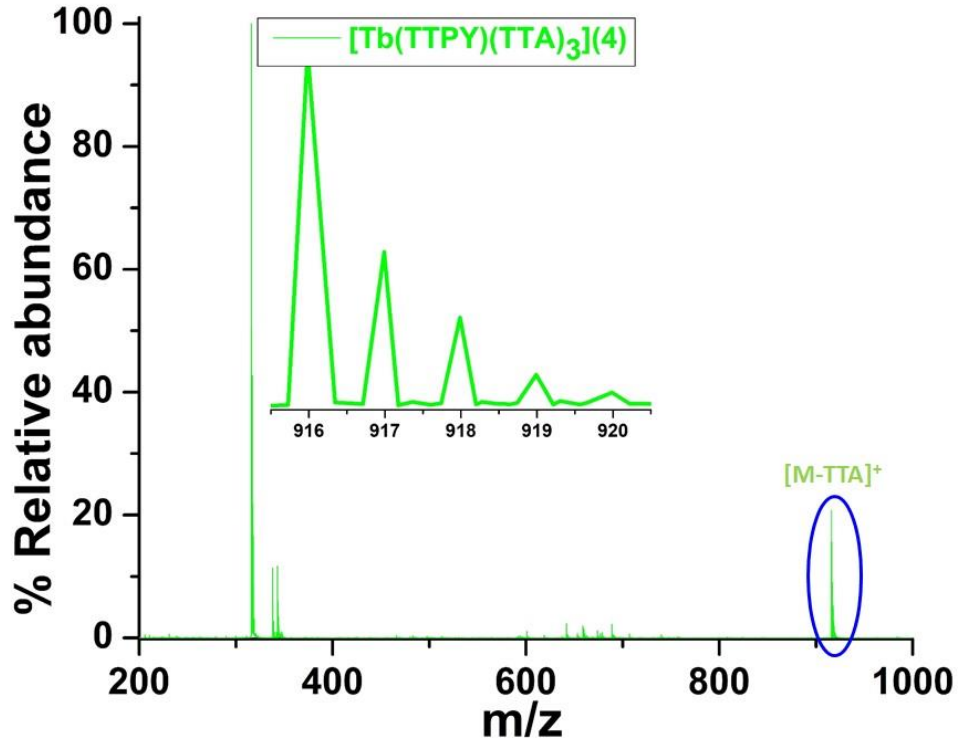

Figure S4. ESI-MS spectra with isotopic distribution for the parent ion peak of complex **4** in DMF.

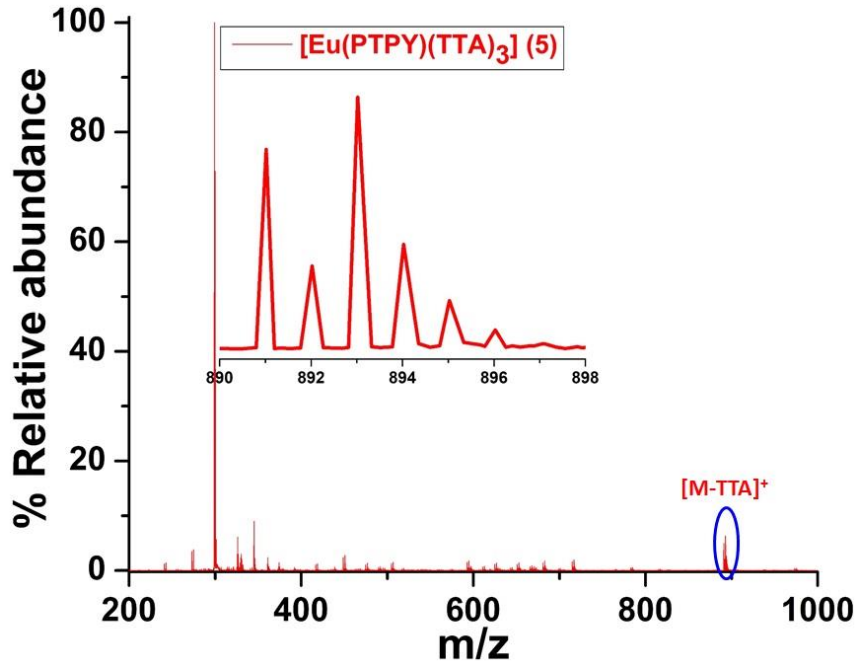

Figure S5. ESI-MS spectra with isotopic distribution for the parent ion peak of complex **5** in DMF.

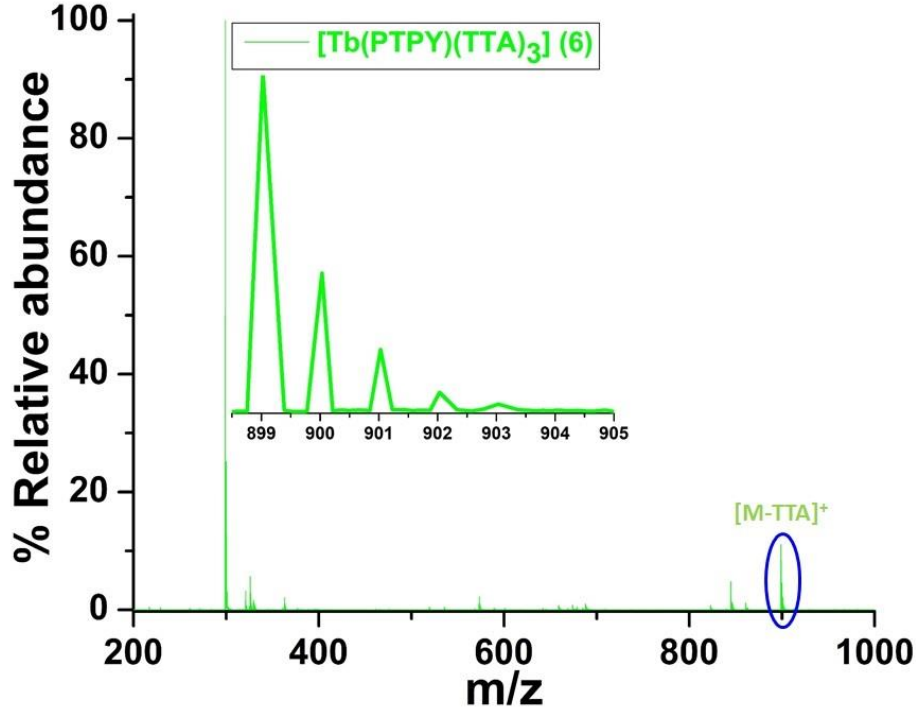

Figure S6. ESI-MS spectra with isotopic distribution for the parent ion peak of complex **6** in DMF.

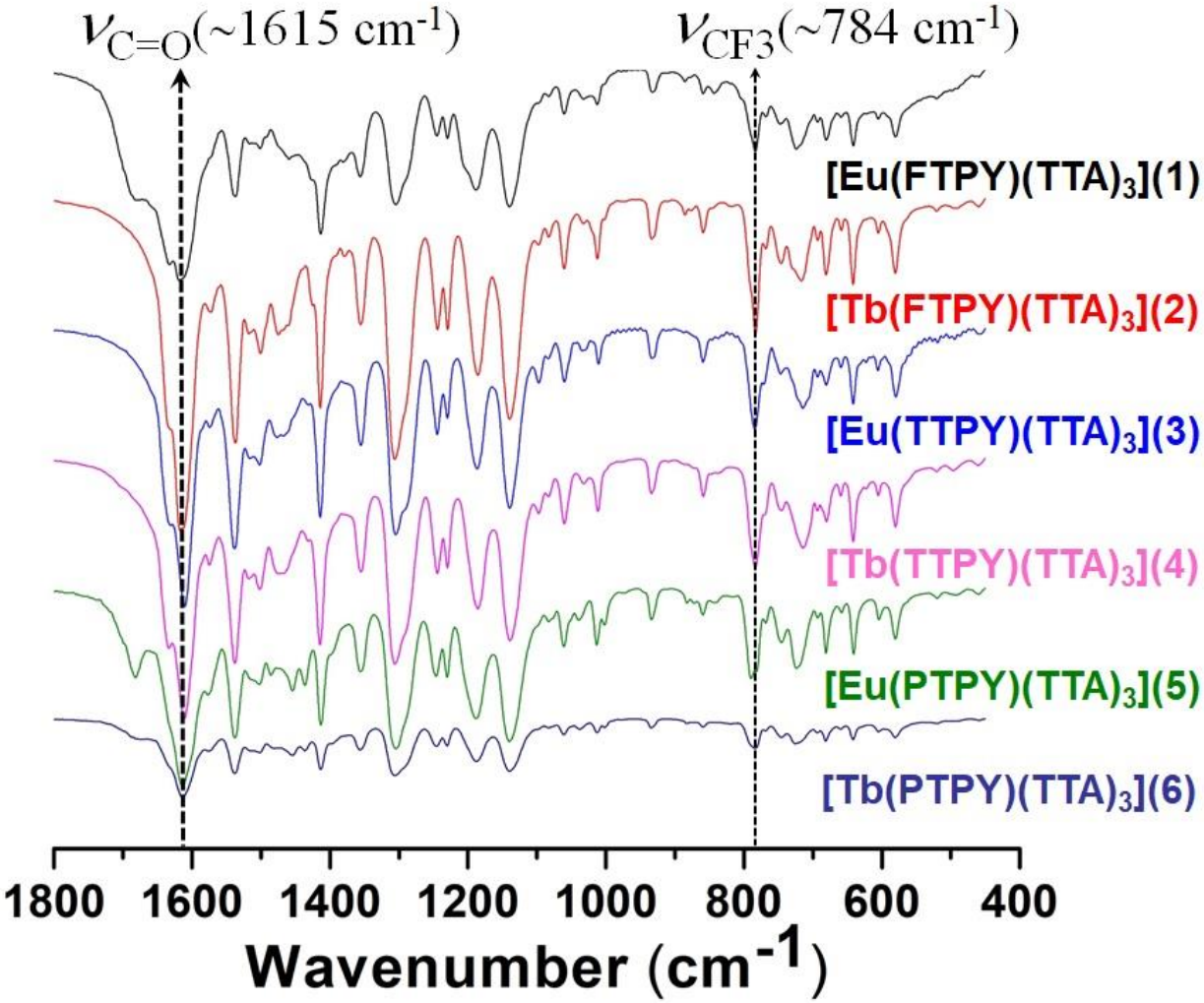

Figure S7. FT-IR spectra of complexes **1-6** (from top to bottom) with matching vibration bands in solid state using KBr disc in fingerprint region in the range of 450-1800 cm^{-1} showing analogous structural features across the series in solid state.

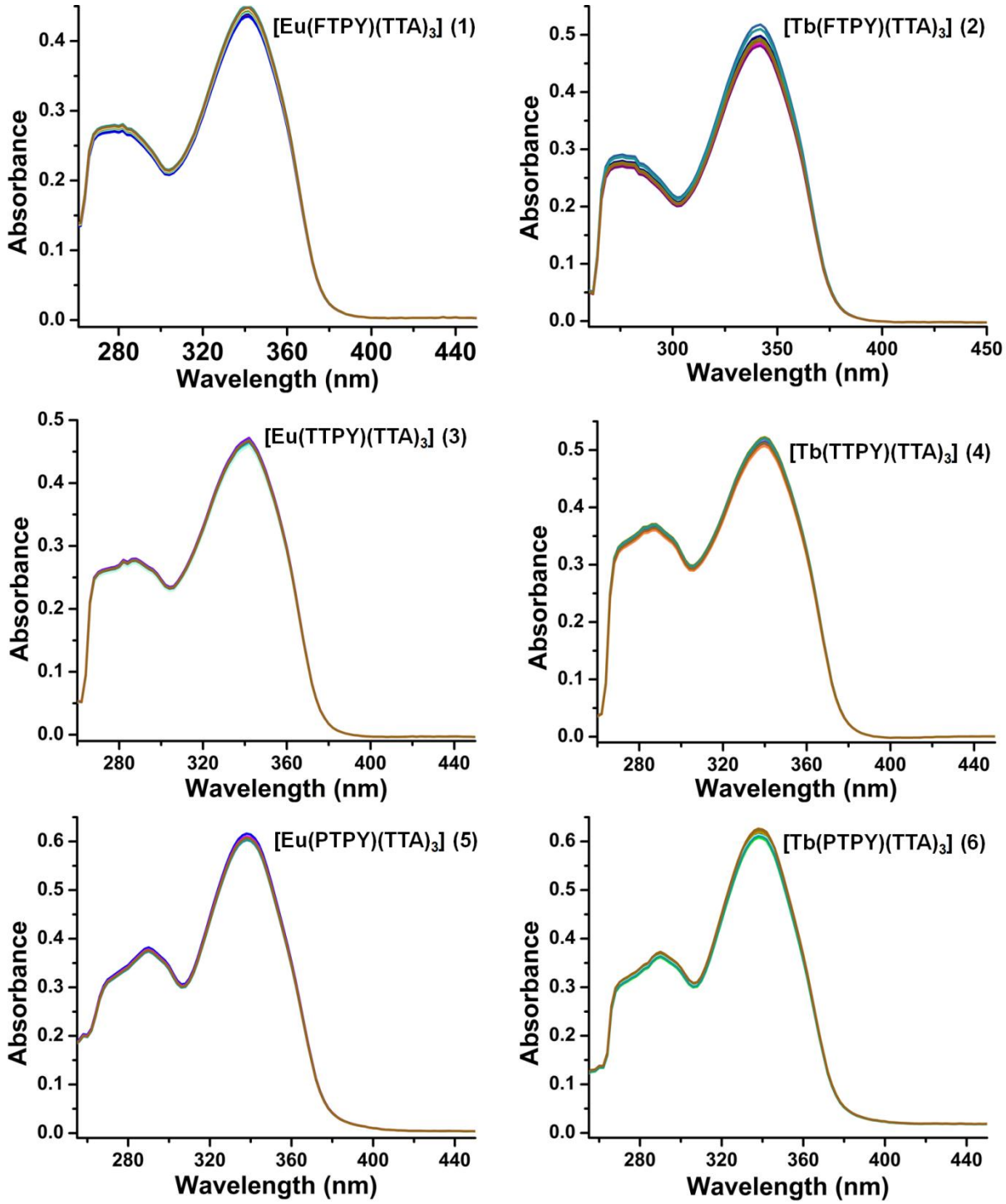

Figure S8. Time-dependent absorption spectral traces of complexes **1-6** recorded for 4 h in every 20 minute time interval in DMF (6 μM) at 298 K to access the stability of the complexes in solution.

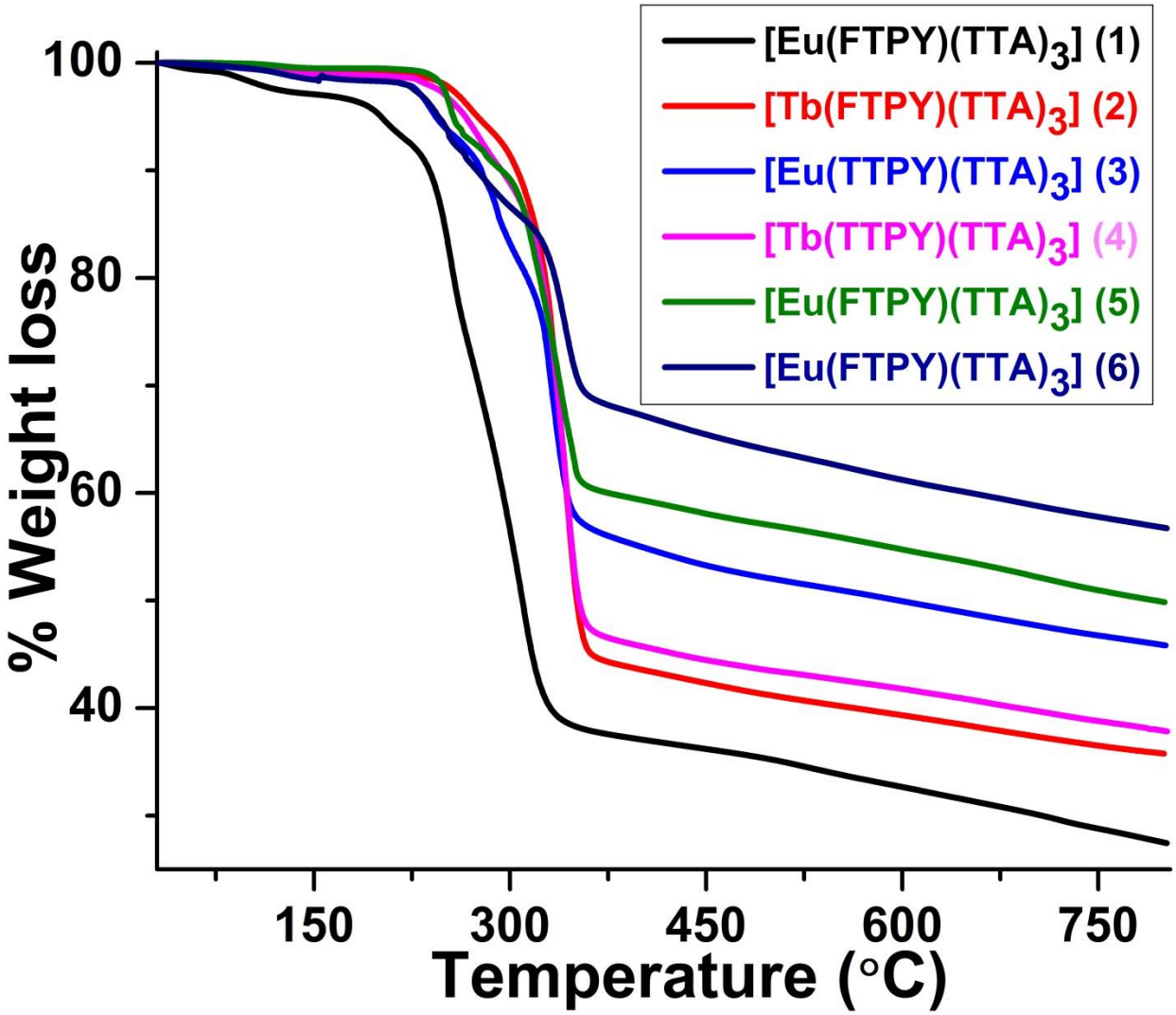

Figure S9. TGA plot of the complexes **1-6** at a heating rate of 10 °C min^{-1} under N_2 atmosphere.

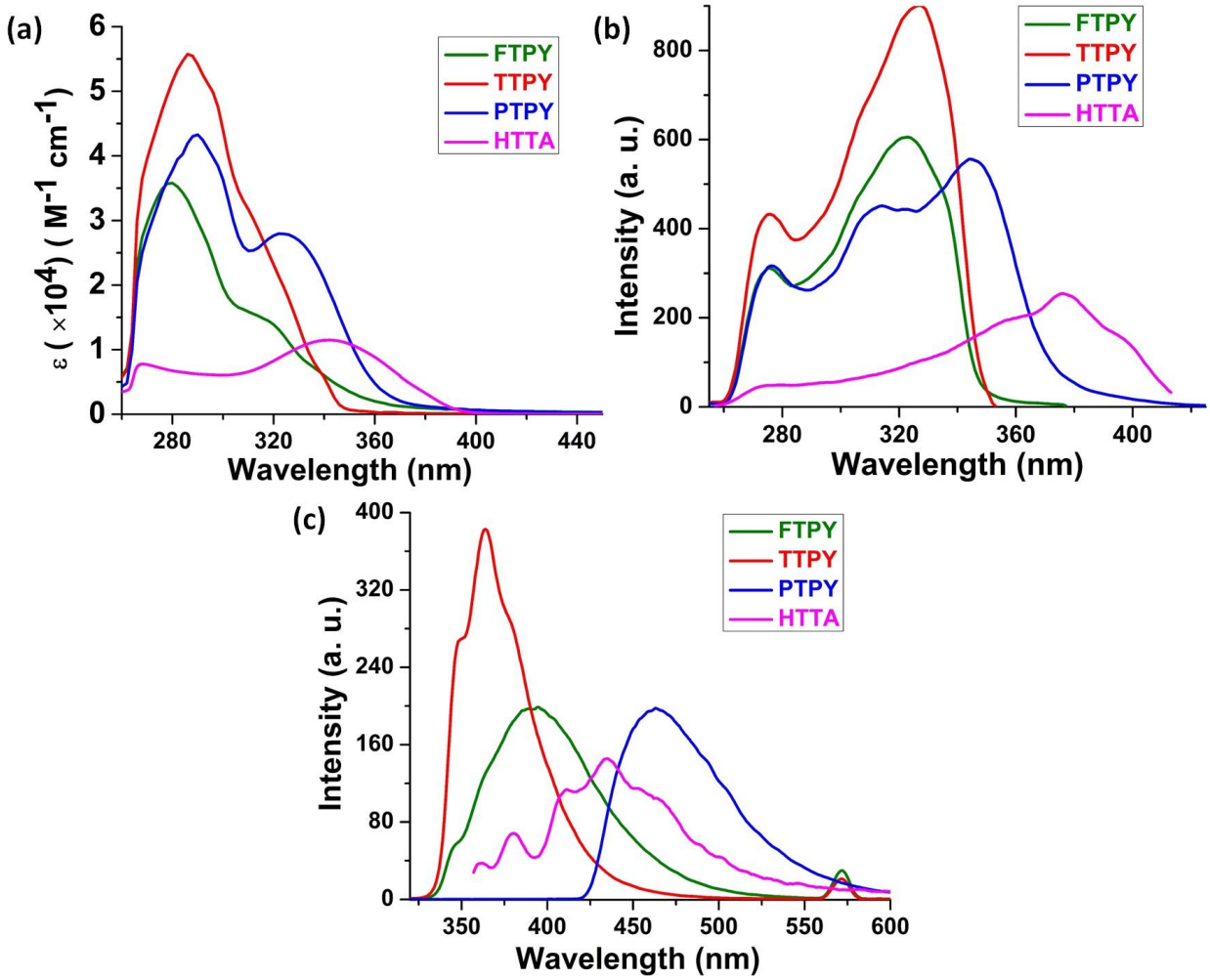

Figure S10. (a) Electronic absorption spectra of R-TPY (14 μM) and HTTA (80 μM) ligands and **(b)** Excitation and **(c)** emission spectra of the R-TPY (28 μM) and HTTA (25 μM) ligands in DMF at 298 K.

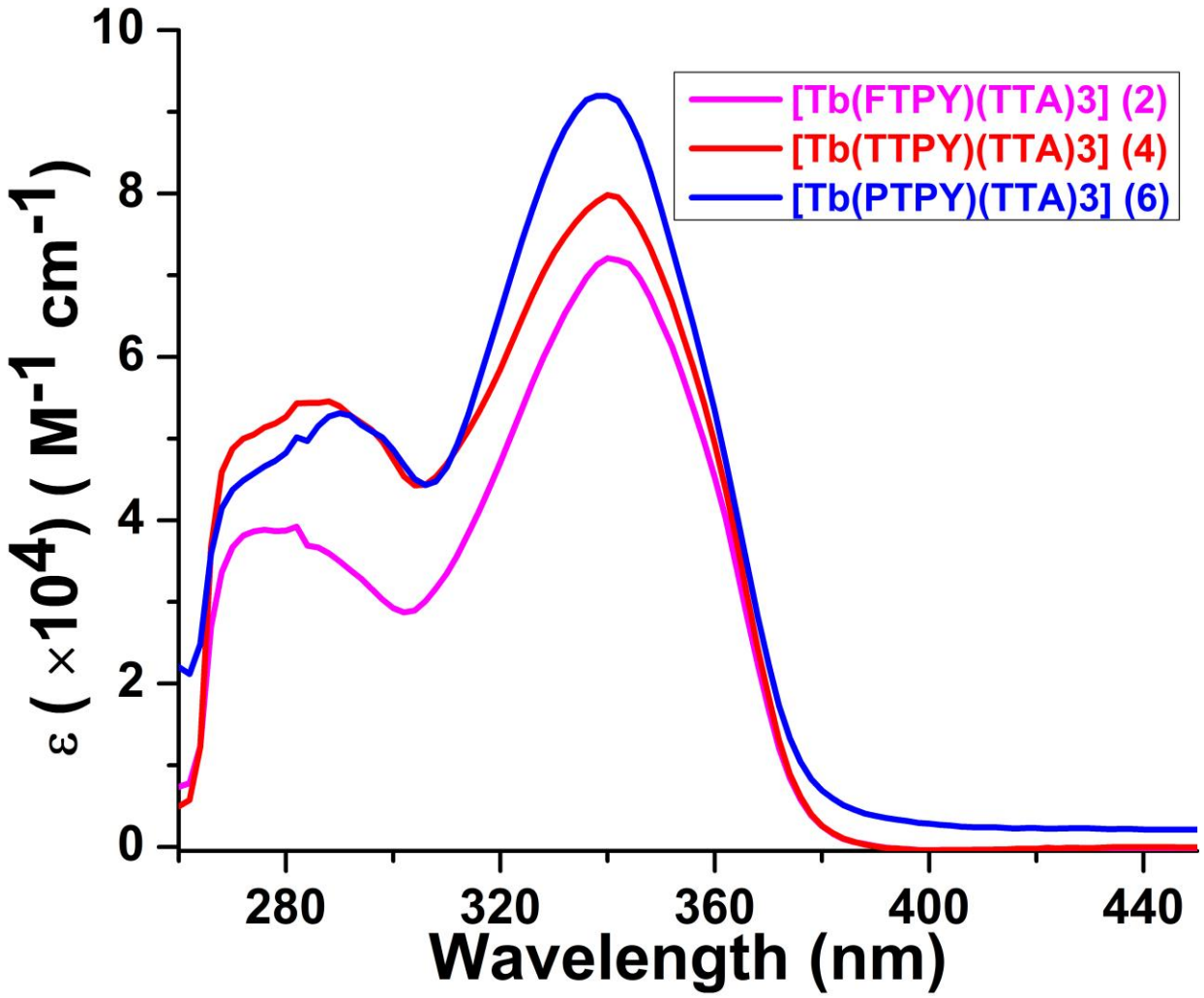

Figure S11. UV-Vis absorption spectral traces of Complexes **2, 4** and **6** in DMF (6 μM) at 298 K.

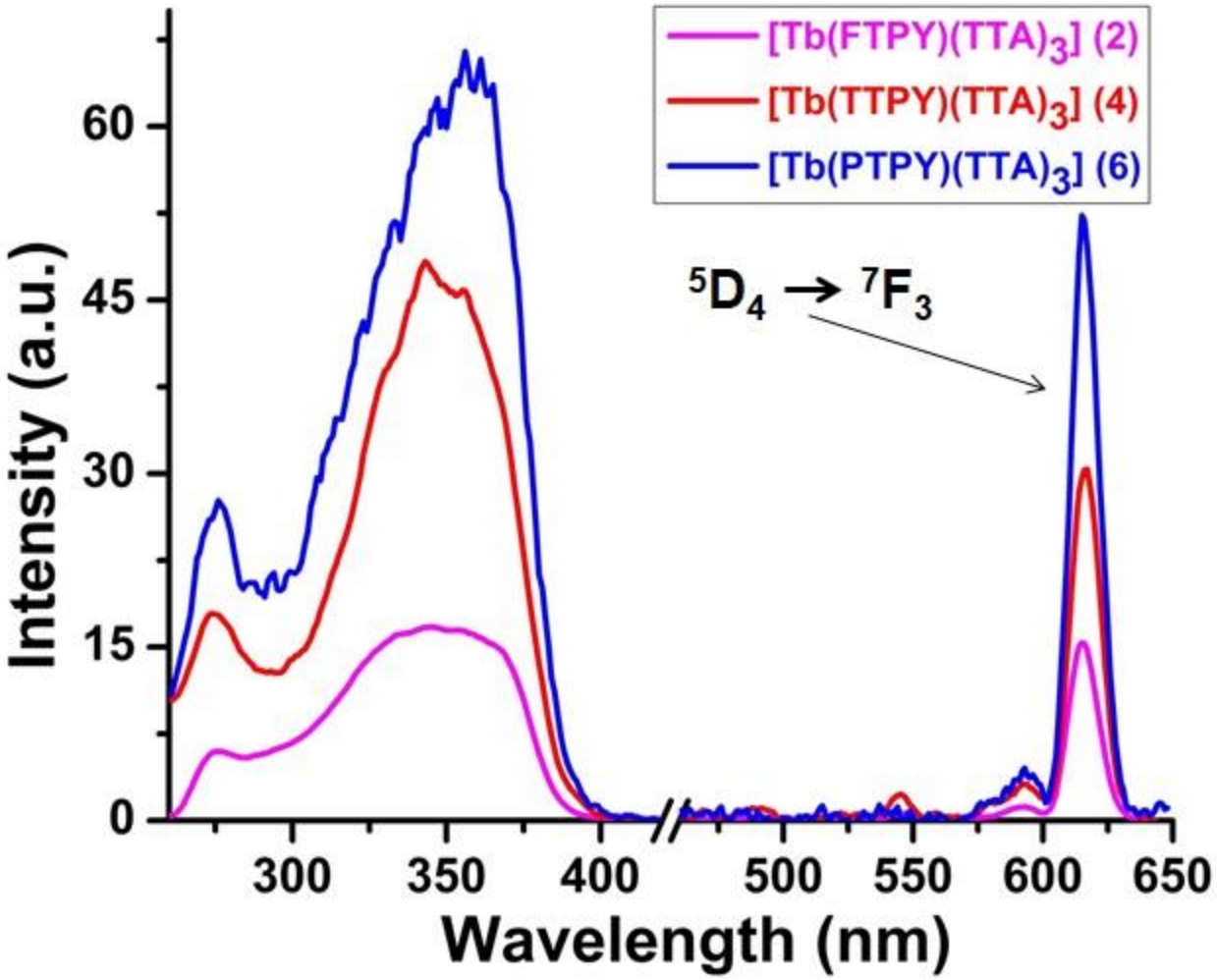

Figure S12. Excitation spectra and time-delayed luminescence spectra for Tb-complexes **2, 4** and **6** in DMF (14 μM) at 298 K. [λ_{ex} = 340 nm, slit width = 5 nm].

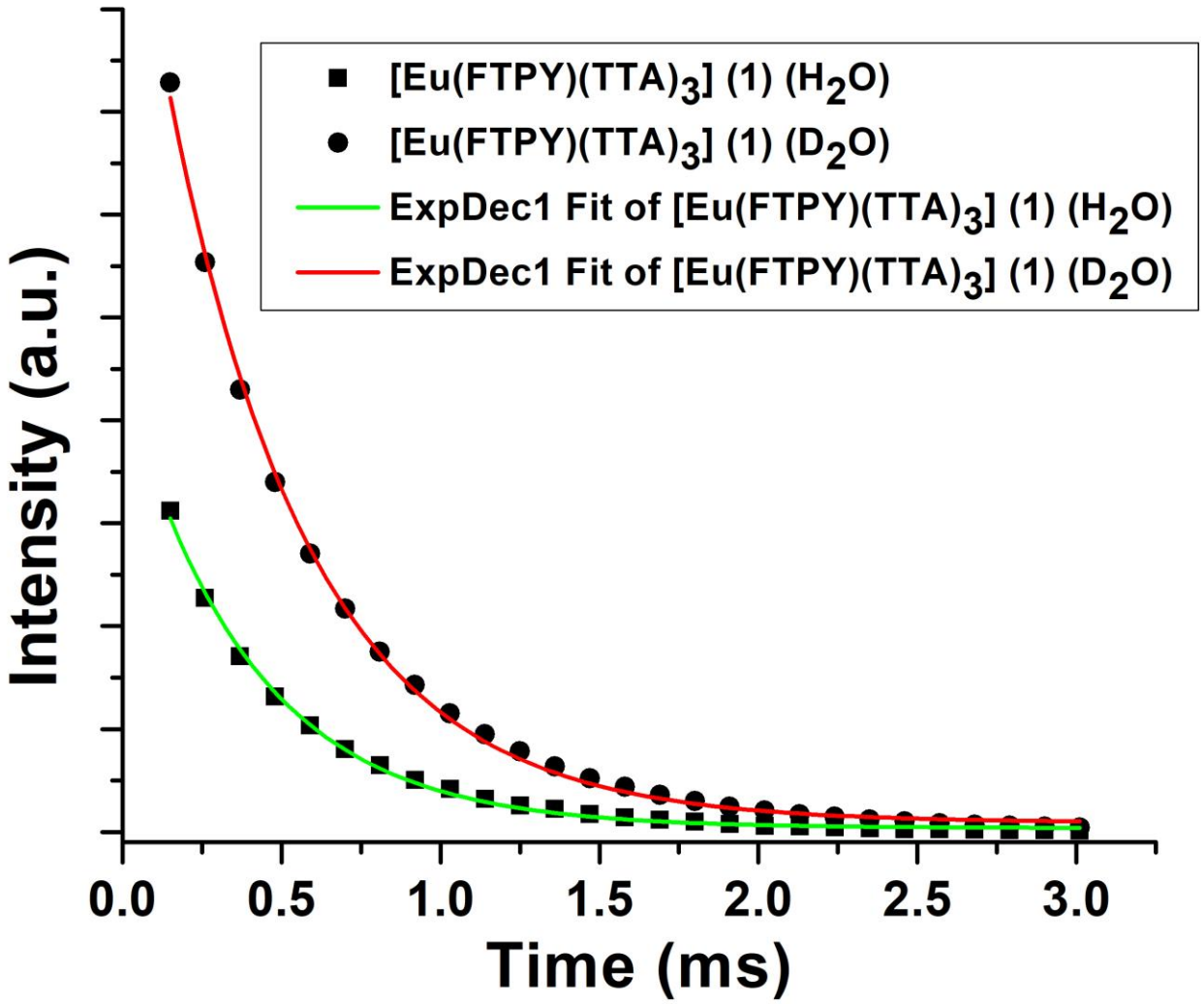

Figure S13: Luminescence decay profile from $^5D_0 - {}^7F_2$ states and lifetime measurements at 615 nm for Eu^{III} complex **1** in H_2O and D_2O (25 μM) at 298 K. λ_{ex}= 340 nm, delay time and gate time = 0.1 ms, total decay time = 3.0 ms, Ex. and Em. Slit width = 5 nm.

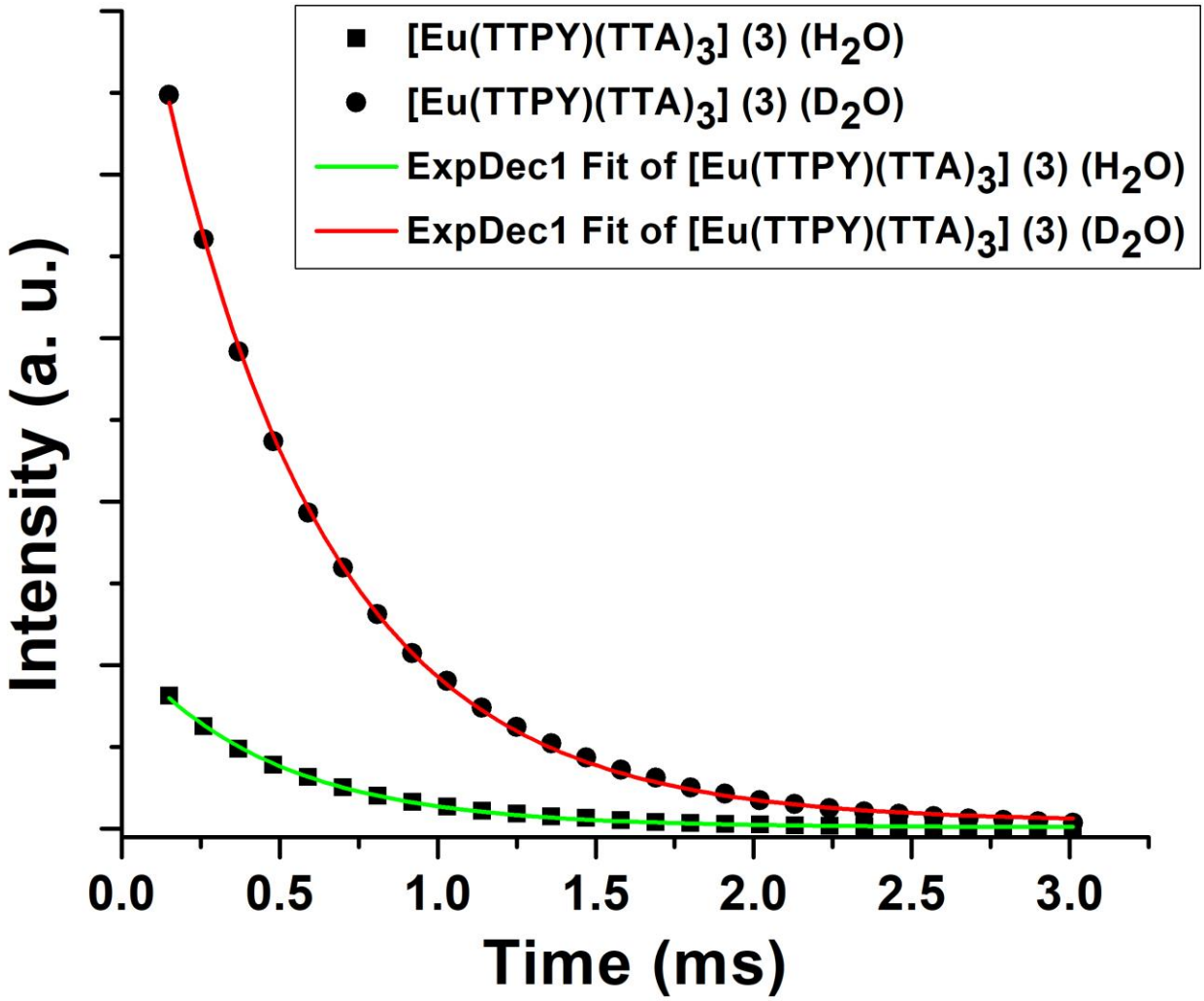

Figure S14: Luminescence decay profile from $^5D_0 - {}^7F_2$ states and lifetime measurements at 615 nm for Eu^{III} complex **3** in H_2O and D_2O (25 μM) at 298 K. λ_{ex}= 340 nm, delay time and gate time = 0.1 ms, total decay time = 3.0 ms, Ex. and Em. Slit width = 5 nm.

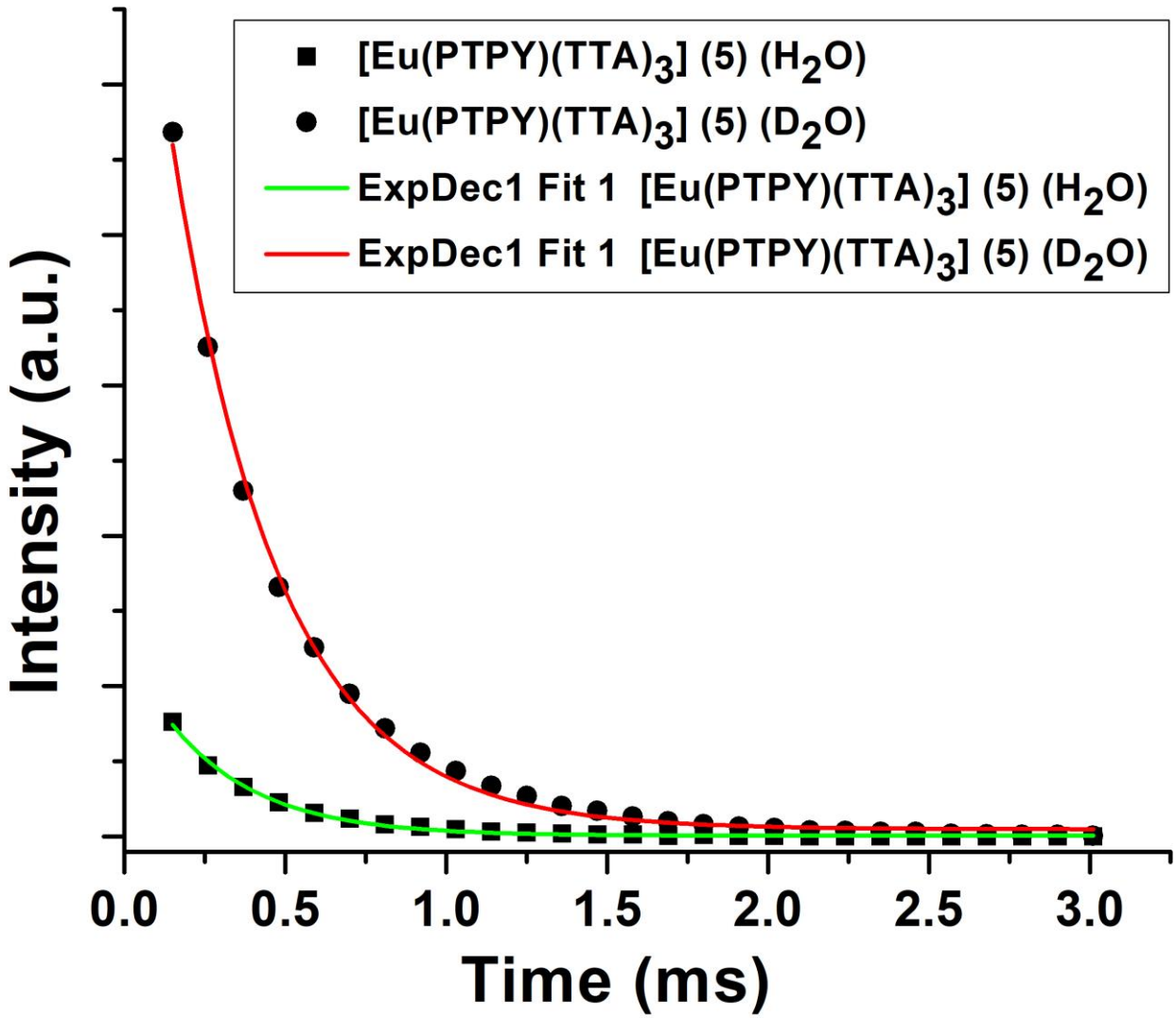

Figure S15: Luminescence decay profile from $^5D_0 - {}^7F_2$ states and lifetime measurements at 615 nm for Eu^{III} complex **5** in H_2O and D_2O (25 μM) at 298 K. λ_{ex}= 340 nm, delay time and gate time = 0.1 ms, total decay time = 3.0 ms, Ex. and Em. Slit width = 5 nm.

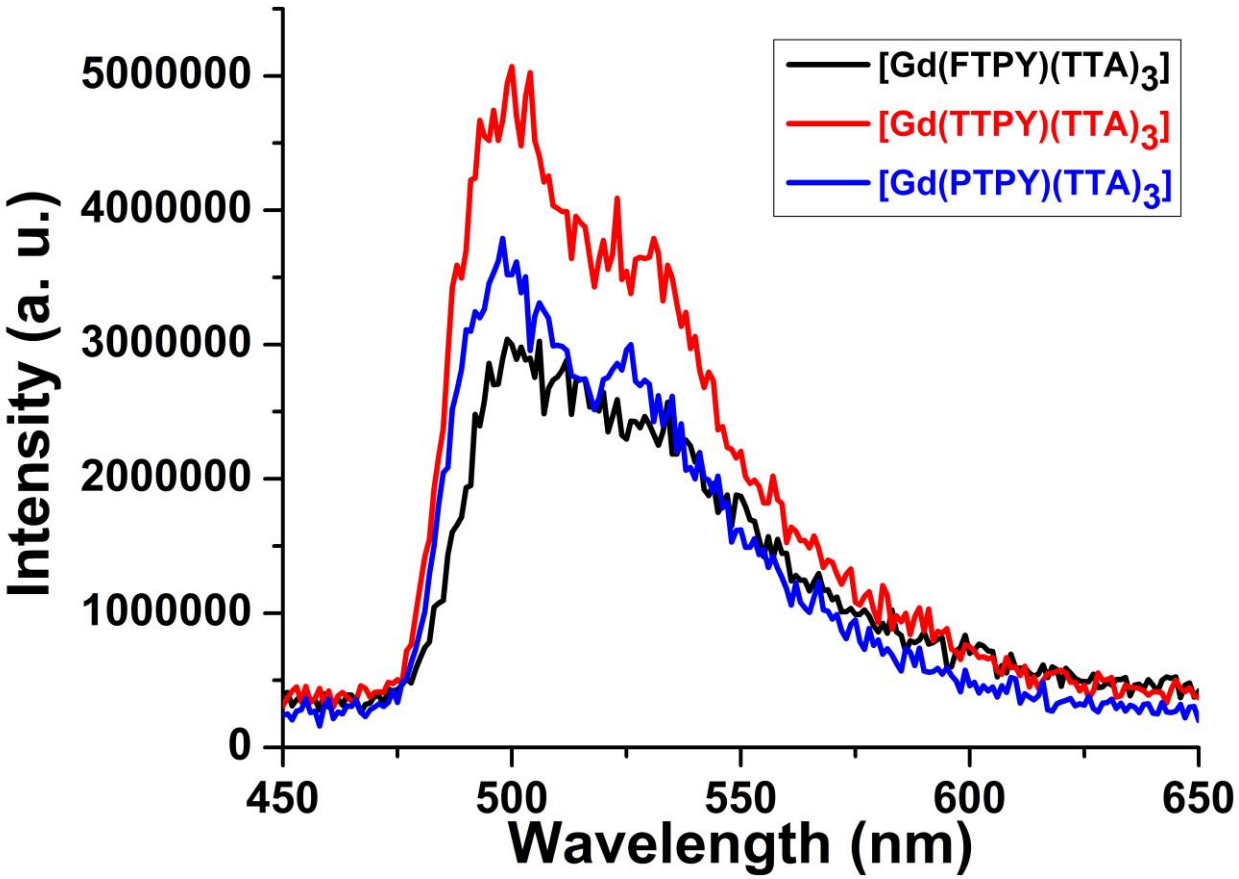

Figure S16. Phosphorescence spectra of [Gd(RTPY)(TTA)$_3$] in DMF(200 μM) at 77 K. [λ_{ex} = 340 nm, slit width = 2.5 nm]

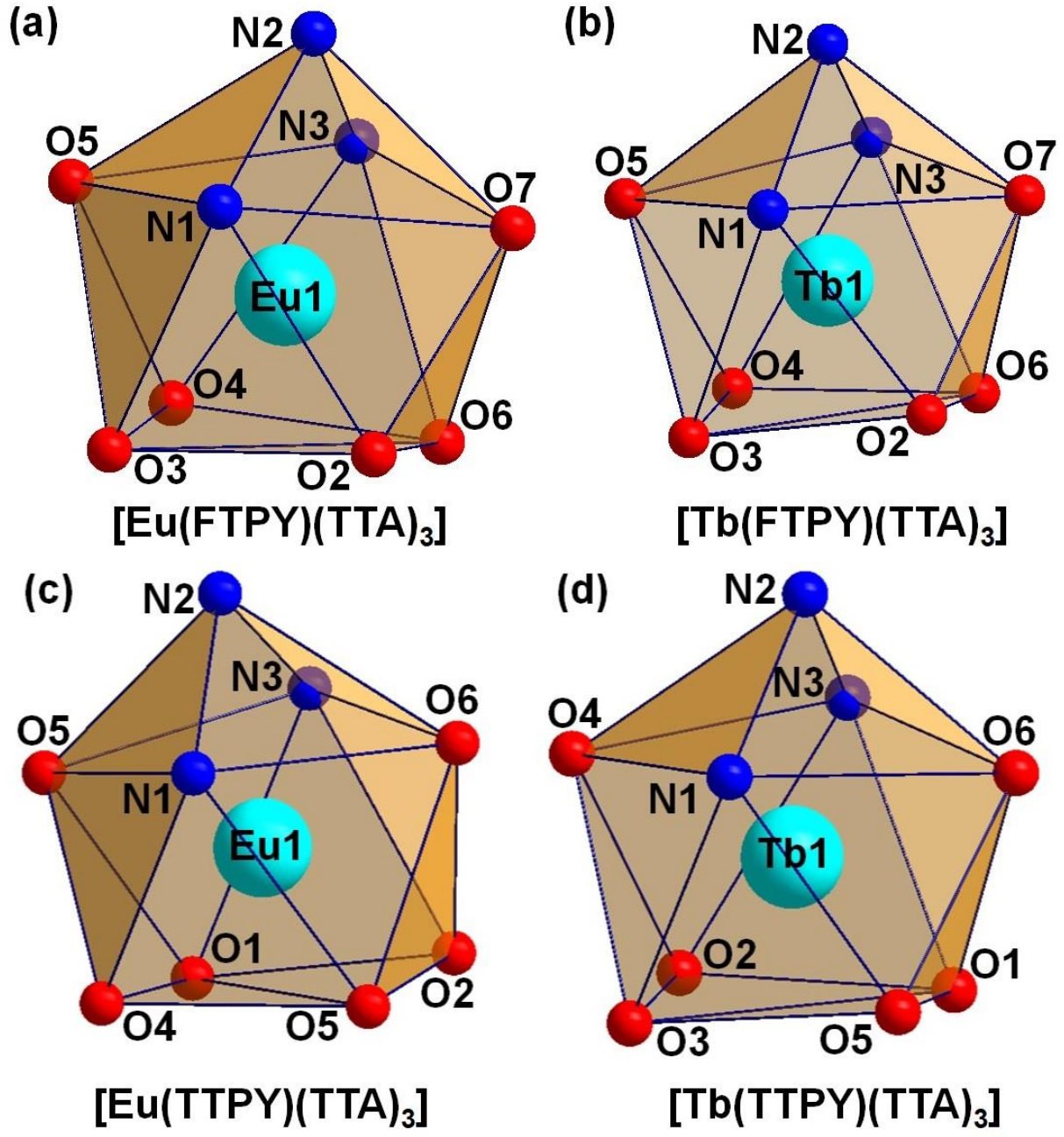

Figure S17. Coordination polyhedra of the lanthanide cores for the complexes (**1-4**) showing tricapped trigonal prismatic geometry**.**

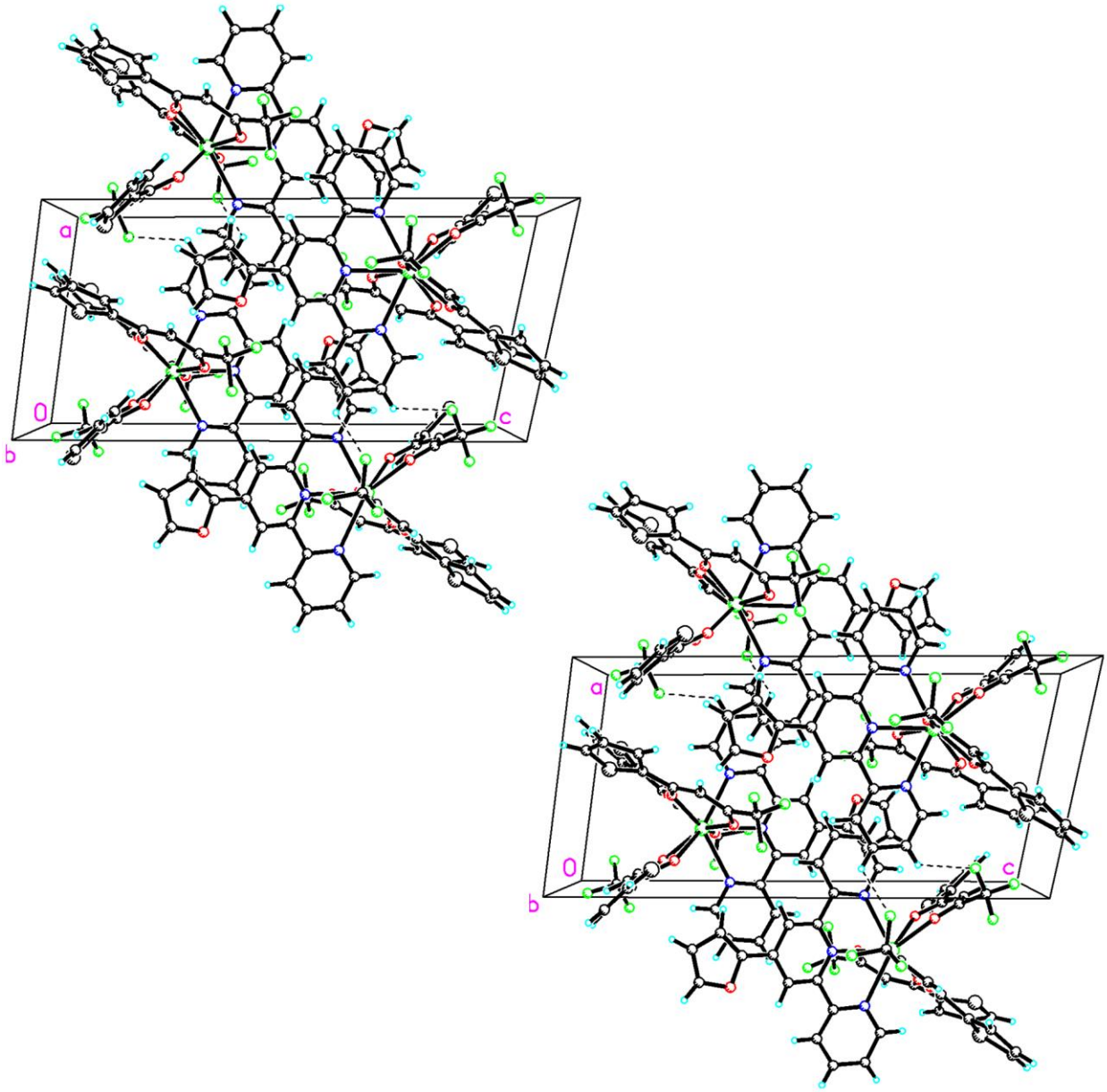

Figure S18. Unit cell packing diagram of Complex **1** (top) and **3** (bottom) viewed along b axis.

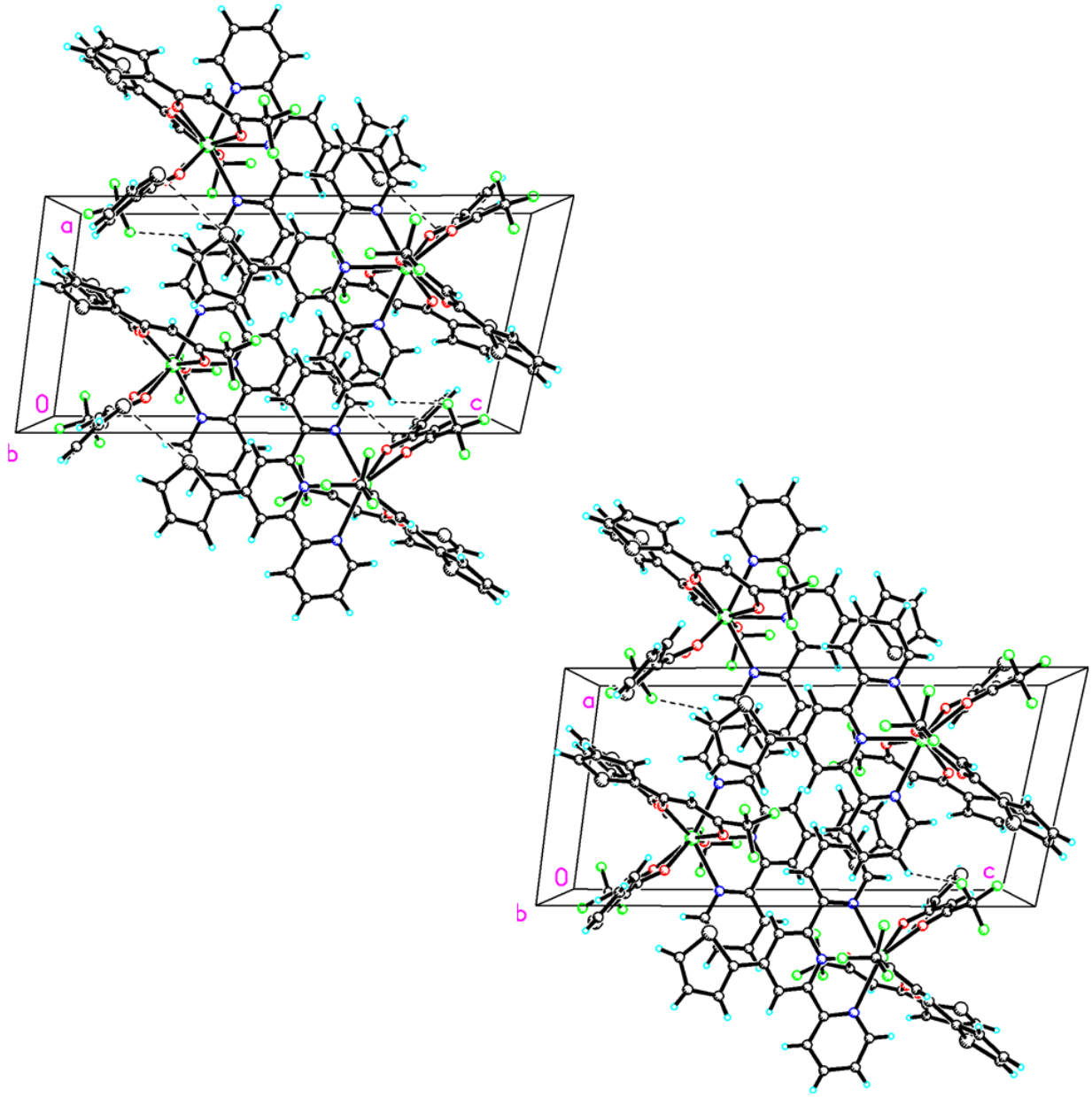

Figure S19. Unit cell packing diagram of Complex **2** (top) and **4** (bottom) viewed along b axis.

Table S1: Selected bond lengths (Å) and bond angles (deg) for [Eu(FTPY)(TTA)$_3$] (**1**), [Tb(FTPY)(TTA)$_3$] (**2**), [Eu(TTPY)(TTA)$_3$] (**3**) and [Tb(TTPY)(TTA)$_3$] (**4**).

Bond length (Å)	(**1**) Ln = Eu	(**2**) Ln = Tb	**Bond length (Å)**	(**3**) Ln = Eu	(**4**) Ln = Tb
Ln(1)-O(2)	2.448(4)	2.426(5)	Ln(1)-O(1)	2.448(5)	2.416(4)
Ln(1)-O(3)	2.406(4)	2.366(5)	Ln(1)-O(2)	2.409(6)	2.386(5)
Ln(1)-O(4)	2.385(4)	2.365(5)	Ln(1)-O(3)	2.396(5)	2.369(5)
Ln(1)-O(5)	2.404(4)	2.376(5)	Ln(1)-O(4)	2.394(5)	2.374(4)
Ln(1)-O(6)	2.399(4)	2.372(5)	Ln(1)-O(5)	2.390(6)	2.372(4)
Ln(1)-O(7)	2.393(4)	2.367(5)	Ln(1)-O(6)	2.414(5)	2.365(4)
Ln(1)-N(1)	2.580(5)	2.563(6)	Ln(1)-N(1)	2.608(7)	2.597(6)
Ln(1)-N(2)	2.618(5)	2.586(6)	Ln(1)-N(2)	2.618(6)	2.595(5)
Ln(1)-N(3)	2.609(5)	2.579(7)	Ln(1)-N(3)	2.587(6)	2.556(5)
Bond angle (deg)			**Bond angle (deg)**		
O(2)-Ln(1)-O(3)	69.38(15)	69.87(18)	O(1)-Ln(1)-O(2)	69.2518)	69.43(15)
O(2)-Ln(1)-O(4)	113.11(15)	112.81(19)	O(1)-Ln(1)-O(3)	68.40(18)	112.69(16)
O(2)-Ln(1)-O(5)	136.85(15)	136.89(18)	O(1)-Ln(1)-O(4)	73.52(18)	136.92(16)
O(2)-Ln(1)-O(6)	68.09(15)	67.86(17)	O(1)-Ln(1)-O(5)	113.13(19)	67.90(15)
O(2)-Ln(1)-O(7)	72.94(14)	72.99(17)	O(1)-Ln(1)-O(6)	136.82(19)	73.56(15)
O(2)-Ln(1)-N(1)	77.27(15)	76.75(18)	O(1)-Ln(1)-N(1)	137.87(19)	137.65(16)
O(2)-Ln(1)-N(2)	127.7(3)	127.75(17)	O(1)-Ln(1)-N(2)	128.14(18)	128.43(15)
O(2)-Ln(1)-N(3)	137.73(18)	137.73(18)	O(1)-Ln(1)-N(3)	77.64(19)	77.53(16)
O(3)-Ln(1)-O(4)	72.90(16)	72.3(2)	O(2)-Ln(1)-O(3)	103.91(19)	72.77(18)
O(3)-Ln(1)-O(5)	71.78(15)	71.71(18)	O(2)-Ln(1)-O(4)	140.76(18)	71.88(15)
O(3)-Ln(1)-O(6)	103.14(15)	102.85(18)	O(2)-Ln(1)-O(5)	72.7(2)	103.63(13)
O(3)-Ln(1)-O(7)	140.53(15)	140.84(18)	O(2)-Ln(1)-O(6)	71.94(18)	140.72(15)
O(3)-Ln(1)-N(1)	78.10(15)	77.64(19)	O(2)-Ln(1)-N(1)	143.1(2)	142.86(17)
O(3)-Ln(1)-N(2)	126.80(16)	126.60(18)	O(2)-Ln(1)-N(2)	127.06(19)	126.61(16)
O(3)-Ln(1)-N(3)	142.90(16)	142.60(19)	O(2)-Ln(1)-N(3)	78.1(2)	77.36(16)
O(4)-Ln(1)-O(5)	71.38(15)	72.17(18)	O(3)-Ln(1)-O(4)	71.60(17)	71.95(16)
O(4)-Ln(1)-O(6)	69.59(15)	69.35(18)	O(3)-Ln(1)-O(5)	70.33(19)	69.86(16)
O(4)-Ln(1)-O(7)	134.81(15)	135.61(19)	O(3)-Ln(1)-O(6)	140.70(18)	135.82(16)
O(4)-Ln(1)-N(1)	142.29(16)	141.93(19)	O(3)-Ln(1)-N(1)	75.7(2)	72.42(18)
O(4)-Ln(1)-N(2)	118.96(15)	119.44(18)	O(3)-Ln(1)-N(2)	128.97(19)	118.87(16)
O(4)-Ln(1)-N(3)	72.30(17)	72.7(2)	O(3)-Ln(1)-N(3)	142.14(19)	141.58(17)

O(5)-Ln(1)-O(6)	140.27(14)	140.80(16)	O(4)-Ln(1)-O(5)	135.6(2)	140.98(15)
O(5)-Ln(1)-O(7)	136.16(14)	135.04(17)	O(4)-Ln(1)-O(6)	135.20(17)	134.61(15)
O(5)-Ln(1)-N(1)	77.05(15)	76.65(18)	O(4)-Ln(1)-N(1)	75.31(19)	85.36(17)
O(5)-Ln(1)-N(2)	65.79(15)	65.26(17)	O(4)-Ln(1)-N(2)	69.54(17)	65.14(15)
O(5)-Ln(1)-N(3)	85.25(16)	85.35(18)	O(4)-Ln(1)-N(3)	82.34(19)	76.21(16)
O(6)-Ln(1)-O(7)	72.53(14)	73.55(17)	O(5)-Ln(1)-O(6)	71.28(19)	73.37(15)
O(6)-Ln(1)-N(1)	141.85(15)	141.53(17)	O(5)-Ln(1)-N(1)	72.6(2)	75.92(16)
O(6)-Ln(1)-N(2)	129.99(16)	130.47(18)	O(5)-Ln(1)-N(2)	118.73(19)	129.68(16)
O(6)-Ln(1)-N(3)	76.21(16)	76.55(19)	O(5)-Ln(1)-N(3)	141.7(2)	142.01(15)
O(7)-Ln(1)-N(1)	82.66(15)	82.31(17)	O(6)-Ln(1)-N(1)	85.3(2)	75.64(16)
O(7)-Ln(1)-N(2)	70.38(15)	69.81(17)	O(6)-Ln(1)-N(2)	65.68(18)	69.50(15)
O(7)-Ln(1)-N(3)	75.56(15)	75.70(18)	O(6)-Ln(1)-N(3)	76.55(19)	82.35(15)
N(1)-Ln(1)-N(2)	62.61(16)	63.19(18)	N(1)-Ln(1)-N(2)	62.6(2)	62.96(17)
N(1)-Ln(1)-N(3)	125.41(16)	126.06(19)	N(1)-Ln(1)-N(3)	125.1(2)	125.96(17)
N(2)-Ln(1)-N(3)	62.99(16)	63.06(19)	N(2)-Ln(1)-N(3)	62.65(19)	63.16(16)

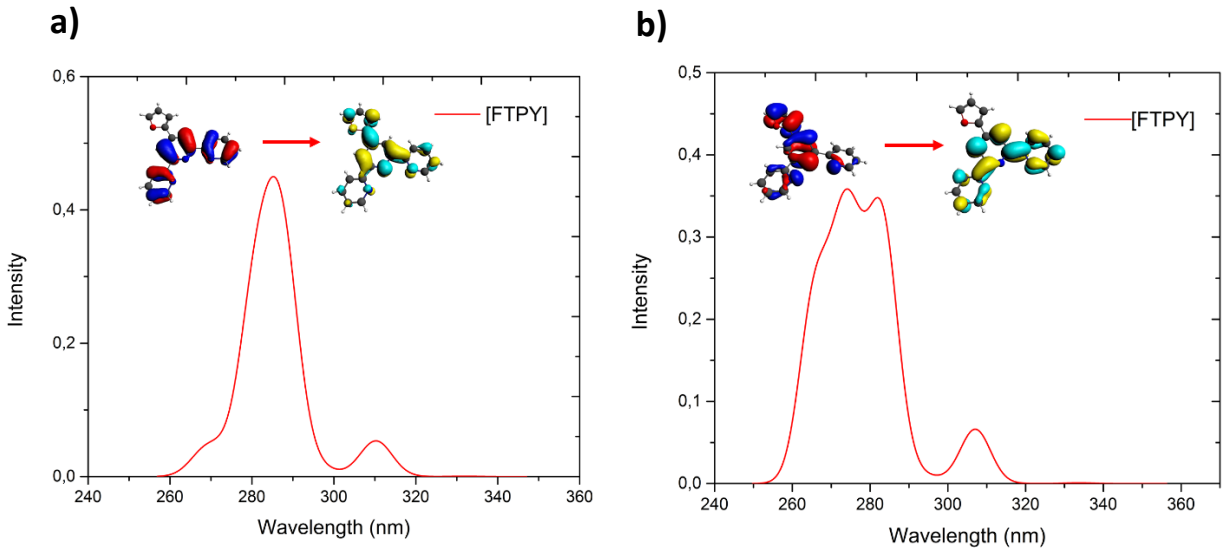

Figure S20. Theoretically predicted Absorption spectra of [FTPY] ligand taken from (a) [Eu(FTPY)(TTA)$_3$] (**1**) and (b) [Tb(FTPY)(TTA)$_3$] (**2**).

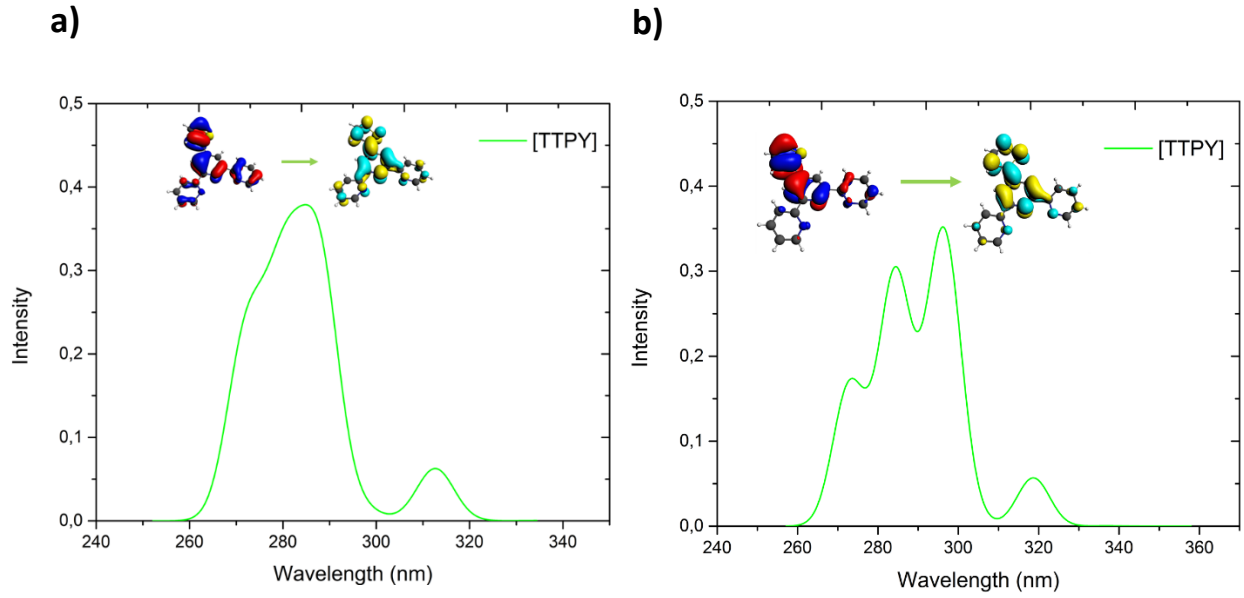

Figure S21. Theoretically predicted Absorption spectra of [TTPY] ligand taken from (a) [Eu(TTPY)(TTA)$_3$] (**3**) and (b) [Tb(TTPY)(TTA)$_3$] (**4**).

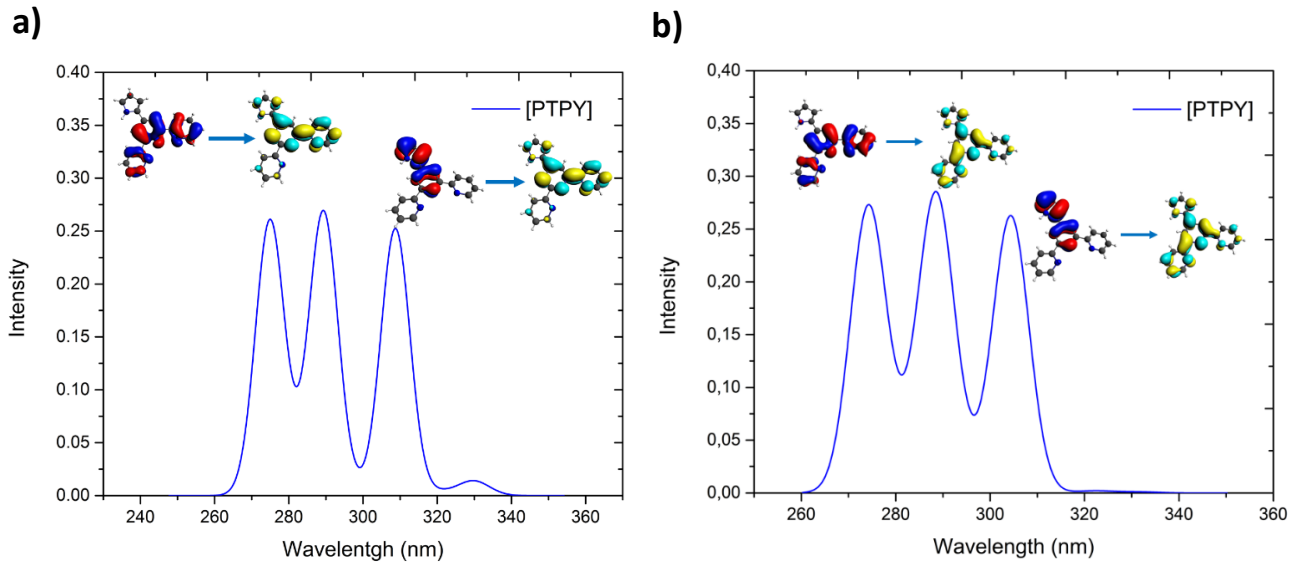

Figure S22. Theoreticlly predicted absorption spectra of [PTPY] ligand taken from (a) [Eu(PTPY)(TTA)$_3$] (**5**) and (b) [Tb(PTPY)(TTA)$_3$] (**6**).

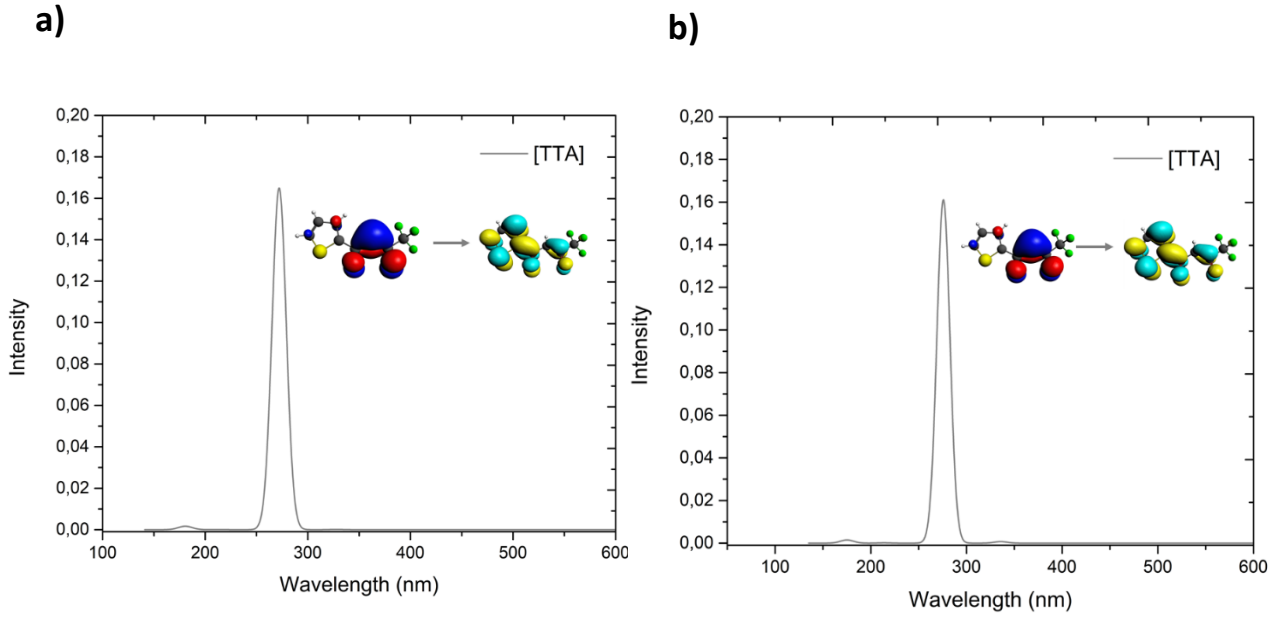

Figure S23. Theoretically predicated absorption spectra of [TTA] ligand taken from a) [Eu(FTPY)(TTA)$_3$] b) [Tb(FTPY)(TTA)$_3$] (**2**).

Table S2. Main electronic transitions for [Eu(FTPY)(TTA)$_3$] (**1**) and [Tb(FTPY)(TTA)$_3$] (**2**) complexes. All values are in cm^{-1}.

Transition	[Eu(FTPY)(TTA)$_3$]	Transition	[Tb(FTPY)(TTA)$_3$]
$^5D_0 \rightarrow {}^7F_0$	18001	$^5D_4 \rightarrow {}^7F_0$	16250
$^5D_0 \rightarrow {}^7F_1$	17583	$^5D_4 \rightarrow {}^7F_1$	16369
$^5D_0 \rightarrow {}^7F_2$	16796	$^5D_4 \rightarrow {}^7F_2$	16729
$^5D_0 \rightarrow {}^7F_3$	15861	$^5D_4 \rightarrow {}^7F_3$	17455
$^5D_0 \rightarrow {}^7F_4$	14740	$^5D_4 \rightarrow {}^7F_4$	18276
$^5D_0 \rightarrow {}^7F_5$	13644	$^5D_4 \rightarrow {}^7F_5$	19678
$^5D_0 \rightarrow {}^7F_6$	12401	$^5D_4 \rightarrow {}^7F_6$	21508

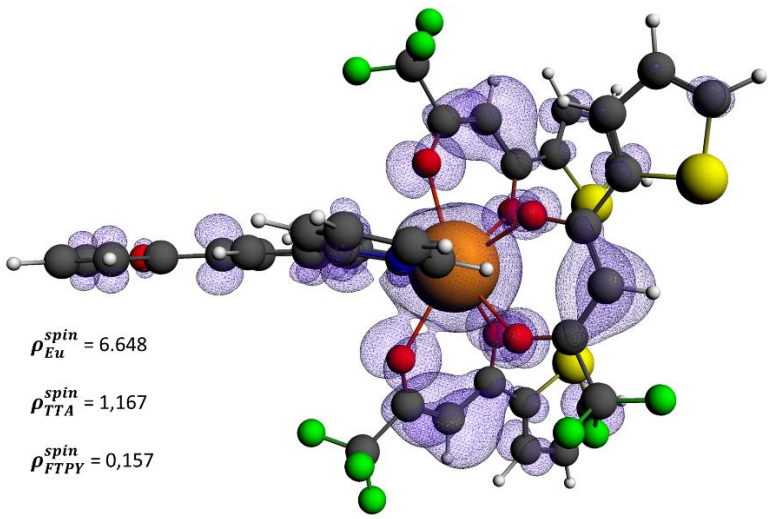

Figure S24. Calculated spin density for the [Eu(FTPY)(TTA)$_3$] (**1**) complex.

Spin Density Calculation: Since the excitation of the ligands at a determined wavelength is performed, a process called intersystem-crossing (ISC) take place allowing to reach the lowest triplet state from which the energy is transferred to the lanthanide ion. To corroborate the results obtained from the CASSCF/NEVPT2 calculations for the determination of the ligand from which the sensitization is produced, the spin density was analyzed. The [Eu(FTPY)(TTA)$_3$] (**1**) complex was taken as a benchmark system for this purpose. Firstly, a geometry optimization was carried

out using the Amsterdam Density Functional (ADF) package.[1] The scalar relativistic effects were incorporated by means of a two-component Hamiltonian with the zeroth-order regular approximation (ZORA).[2] The BP86 generalized gradient approximation exchange-correlation functional was employed with the standard Slater-type orbital (STO) basis set and the triple-ξ quality double plus polarization function (TZVP) for all the atoms.[3] To consider the sensitizer ligand in its triplet state, the spin polarization ($\Delta\rho$) was established to 8 which corresponds to the sum of $\Delta\rho = 6$ and $\Delta\rho = 2$ contributed by Eu^{III} ion (septuplet) and the ligand (triplet), respectively.

As expected, the spin-density plot exhibited in Figure S14 shows that the greatest contribution comes from the Eu^{III} ion with a ρ^{spin} value close to 6. The remaining density is mainly located on the TTA ligands evidencing, from an energetic point of view, that these ligands probably sensitize the lanthanide center, as predicted by the multiconfigurational methods. On the basis of previous calculations exhibited in this work which did not show significant differences between the systems under study, this result could be extended to the other Eu-compounds.

References

1. E. J. Baerends, T. Ziegler, J. Autschbach, D. Bashford, A. Berces, F. M. Bickelhaupt, C. Bo, L. Cavallo, D. P. Chong, L. Deng, R. M. Dickson, D. E. Ellis, L. Fan, C. F. Guerra, A. Ghysels, A. Giammona, O. V. Gritsenko, S. Gusarov, F. E. Harris, C. R. Jacob, L. Jensen, J. W. Kaminski, F. Kootstra, A. Kovalenko, M. V. Krykunov, D. A. McCormack, A. Michalak, M. Mitoraj, J. Neugebauer, V. P. Nicu, L. Noodleman, S. Patchkovskii, P. H. T. Philipsen, D. Post, C. C. Pye, W. Ravenek, P. Ros, G. Schreckenbach, M. Seth, J. G. Snijders, L. Vernooijs, L. Versluis, O. Visscher, F. Visser, T. A. Wang, E. M. van Wesolowski, G. Wezenbeek, S. K. Wiesenekker, T. K. Wol and A. L. Y. Woo, *Amsterdam Density Functional*; SCM, Theoretical Chemistry, Vrije Universiteit, Amsterdam, The Netherlands, 2012, http://www.scm.com.
2. (a) E. van Lenthe, E. J. Baerends and J. G. Snijders, *J. Chem. Phys.*, 1993, **99**, 4597−4610; (b) F. Wang, G. Hong and L. Li, *Chem. Phys. Lett.*, 2000, **316**, 318−323.
3. (a) J. P. Perdew and W. Yue, *Phys. Rev. B: Condens. Matter Mater. Phys.*, 1986, **33**, 8800; (b) E. van Lenthe and E. J. Baerends, *J. Comput. Chem.*, 2003, **24**, 1142−1156.